Probing nuclear dissipation via evaporation residue excitation functions for the ^{16,18}O + ^{198}Pt reactions

Rohit Sandal,[*] B. R. Behera,[†] Varinderjit Singh,[‡] Maninder Kaur, A. Kumar, Gurpreet Kaur, and P. Sharma
Department of Physics, Panjab University, Chandigarh 160014, India

N. Madhavan, S. Nath, J. Gehlot, A. Jhingan, and K. S. Golda
Inter University Accelerator Centre, Aruna Asaf Ali Marg, New Delhi 110067, India

Hardev Singh
Department of Physics, Kurukshetra University, Kurukshetra 136119, India

S. Mandal and S. Verma
Department of Physics and Astrophysics, Delhi University, Delhi 110007, India

E. Prasad[§]
Department of Physics, Central University of Kerala, Kasaragod 671314, India

K. M. Varier
Department of Physics, University College, Palayam, Thiruvanthapuram 695024, Kerala, India

A. M. Vinodkumar
Department of Physics, University of Calicut, Calicut 673635, India

A. Saxena
Nuclear Physics Division, Bhabha Atomic Research Centre, Mumbai 400085, India

Jhilam Sadhukhan
Variable Energy Cyclotron Centre, 1/AF, Bidhan Nagar, Kolkata 700064, India

Santanu Pal[‖]
CS-6/1 Golf Green, Kolkata 700095, India

Evaporation residue (ER) cross sections for the ^{16,18}O + ^{198}Pt reactions are measured in order to investigate fission hindrance. Compound nuclei (^{214,216}Rn) are formed in the above fusion reactions at excitation energies in the range of 40–68 MeV. The experimental ER cross sections are compared with predictions from the statistical model calculations of compound nuclear decay where Kramers' fission width is used. The strength of nuclear dissipation is treated as a free parameter in the statistical model calculations in order to fit the experimental data.

PACS number(s): 25.70.Gh, 24.10.Pa, 25.70.Jj

I. INTRODUCTION

Evaporation residues (ER) in heavy ion induced fusion-fission reactions are formed as the outcome of competition between fission and various particles and γ evaporation channels of the compound nucleus (CN). Since ER cross sections depend upon the relative magnitude of the fission probability of the compound nucleus with respect to the other CN decay probabilities, they serve as a sensitive probe to investigate fission dynamics particularly in the pre-saddle region [1,2]. ER cross sections for heavy systems are also an important indicator to the possibility of formation of superheavy elements as ERs in fusion reactions [3]. ER cross sections have therefore been measured for a number of compound nuclei in the mass region $\sim$200 and above where fission is an important decay channel.

One of the interesting features of heavy ion induced fusion-fission reactions is the observation [4] that for CN at high excitation energies (temperature > 1 MeV), pre-scission

———————
[*]Present address: S V Govt. College Ghumarwin, Bilaspur 174021 (HP), India.

[†]Corresponding author: bivash@pu.ac.in

[‡]Present address: Department of Chemistry and Center for the Exploration of Energy and Matter, Indiana University, Bloomington, IN 47405, USA.

[§]Present address: Department of Nuclear Physics, Australian National University, Canberra, ACT 2601, Australia.

[‖]Formerly with Variable Energy Cyclotron Centre, Kolkata, India

multiplicity data of light particles and GDR γs point to a hindrance or slowing down of the fission process compared to that given by the transition-state theory of Bohr and Wheeler [5]. The fission hindrance is usually taken into account in statistical model calculations of CN decay by using Kramers' expression for fission width which considers a dissipative dynamics for fission [6]. However, it is often found that the pre-scission multiplicities (of evaporated particles and γ's) and ER cross sections cannot be reproduced with the same strength of dissipation [7,8]. A larger value of fission width is found necessary for ER cross sections than those required to fit pre-scission multiplicities. This is reflected in smaller values of dissipation strength obtained from ER studies than those from analyses of pre-scission multiplicity data. For a number of systems, enhancement of fission width is achieved by reducing the height of the liquid drop model (LDM) fission barrier [9,10]. The above observations suggest that improvements in fission modeling are necessary where effects such as the roles of excitation energy and shape (of the CN) dependence of dissipation need to be further investigated [7]. Experimental data on both pre-scission multiplicities and ER cross sections of a large number of systems are therefore required for a better understanding of the fission process of heavy nuclei with large excitation energies. With this view, we measure the excitation functions of ER cross sections for the reactions ^{16,18}O + ^{198}Pt in the present work. The pre-scission neutron multiplicities for the same systems have been reported in an earlier work [11]. We perform statistical model analysis of the measured ER cross sections using Kramers' fission width where we treat the dissipation strength as a free parameter to fit the ER excitation functions.

The paper is organized as follows. The details of the experimental setup are given in the next section. The data analysis is given in Sec. III where the experimental results are also presented. Section IV contains the statistical model analysis of the data. A summary of the work and discussions are given in the last section.

II. EXPERIMENTAL DETAILS

The experiment [12] was performed at the 15 UD Pelletron accelerator facility of the Inter University Accelerator Centre (IUAC), New Delhi. Pulsed ^{16,18}O beams with a pulse separation of 4 μs (as ERs, produced at the target chamber, took about 3.5 to 4 μs to reach the focal plane, covering a distance of 7.6 m) was used in the experiment to bombard isotopically enriched ^{194}Pt and ^{198}Pt targets of thickness 260 μg/cm^2 and 170 μg/cm^2 each on 10 μg/cm^2 thick carbon backing, respectively. ER excitation function measurements were performed at laboratory beam energies (after correcting for the loss in the pressure window foil of carbon having thickness 660 μg/cm^2 and half thickness of the targets) of 78.0 to 105.6 MeV for the ^{16}O beam and 77.8 to 105.4 MeV for ^{18}O. In addition, ER cross sections were also measured at one energy for the ^{16}O + ^{194}Pt reaction, for which data of ER excitation functions already exist [13], and this data was used for normalization and to obtain the transmission efficiency of the HYbrid Recoil mass Analyzer (HYRA). The heavy ERs produced in the reaction were separated from the
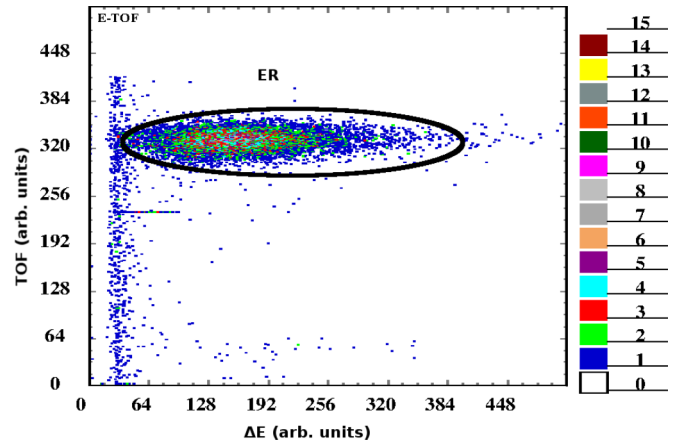
FIG. 1. (Color online) Cathode (ΔE) vs TOF spectrum for ^{16}O + ^{198}Pt at 98.4 MeV.

intense beam background by the gas filled separator HYRA [14]. It is a dual-mode, dual-stage recoil mass separator and spectrometer. The present experiment was performed using the first stage of HYRA in the gas-filled mode. The electromagnetic configuration of the same is Q1Q2-MD1-Q3-MD2-Q4Q5 where Q stands for magnetic quadrupoles and MD stands for magnetic dipoles, respectively.

Elastically scattered oxygen ions were detected in two silicon surface barrier detectors placed at $\pm 22.7^o$ with respect to the beam direction at a distance of 24.5 mm from target for monitoring and normalization of beam flux. The helium gas pressure in HYRA was set at 0.15 torr and HYRA magnetic field settings were calculated using a simulation program [15]. Low-energy ERs reaching the focal plane were detected using a position-sensitive multiwire proportional counter (MWPC) having active area of 152.4 × 50.8 mm^2. The MWPC was operated with isobutane gas of about 2 mbar pressure and it provide position signals (both X and Y positions), an energy signal from the cathode, and a timing signal from the anode. The position signals were taken from the two ends of the X and Y frames through delay-line chips. These were processed through constant fraction discriminators and were fed to the time-to-digital converter as stop signals, with the anode timing as the common start. The data were collected and analyzed using the IUAC data-sorting software CANDLE [16]. At each energy point, magnetic field values were also optimized by maximizing the ER yield at the focal plane, keeping the pressure fixed at 0.15 Torr. To get the time-of-flight (TOF) signal, the start was taken from the focal plane MWPC anode and the stop signal was taken from RF used for beam pulsing. The logical OR signal of the two monitor detectors and the MWPC anode was the master strobe for the data acquisition system. A TOF spectrum was finally generated by taking the start from the MWPC-anode signal and the stop from the RF signal, and was used to effectively separate the ERs reaching the focal plane from other background particles. Figure 1 shows the TOF versus energy spectrum for ^{16}O + ^{198}Pt at 98.4 MeV beam energy. The ERs reaching the focal plane (shown inside the gate) are well separated from other contamination in the above spectrum.

III. DATA ANALYSIS

A. HYRA transmission efficiency

Transmission efficiency of HYRA (T_{eff}) is the ratio of the number of ERs reaching the focal plane to the total number of ERs produced in the target chamber. It depends on various parameters [17], such as the entrance-channel mass asymmetry, beam energy, target thickness, exit channel of interest, the angular acceptance of HYRA, the magnetic field, gas pressure settings of HYRA, and the size of the focal plane detector. Among these parameters, the entrance-channel mass asymmetry, angular acceptance of the separator, target thickness, and the size of the focal plane detector are fixed in a given experiment. The magnetic field values are optimized for maximum yield at the focal plane at each energy. Because the dependence of T_{eff} on gas pressure is found to be rather weak in the energy range of the present study, the same is set at the optimized value (0.15 Torr) throughout the experiment.

The transmission efficiency of a recoil separator is a major concern in ER cross-section measurements, particularly for very asymmetric reactions in normal kinematics. Gas filled separators offer very high transmission efficiency, in comparison with the vacuum mode spectrometers, owing to their inherent velocity and charge-state focusing effects. This feature is particularly useful for studying reactions in which the ER cross section is a small fraction of the total fusion cross section. In the gas medium, particles undergo multiple collisions with the gas molecules, which change the charge state and the energy of the particles. Under optimum field values and pressure, velocity and charge-state focusing take place and the particles traverse a mean trajectory decided by the mean charge state. The mean charge state and the field values of the magnets are calculated using a simulation code [15].

The HYRA transmission efficiency is obtained by using the ER cross-section values for the reaction $^{16}O + ^{194}Pt$ which are already reported [13]. An isotopically enriched ^{194}Pt target of thickness 260 $\mu g/cm^2$ is bombarded by an ^{16}O beam at 96.0 MeV (laboratory) beam energy. As the ER cross section for $^{16}O + ^{194}Pt$ at 96 MeV is known; T_{eff} is obtained for this reaction first. The ER angular distributions for the two reactions are simulated using the semimicroscopic Monte Carlo code TERS [18]. TERS code generates realistic distributions of ER parameters, such as displacement (position), divergence (angle), charge state, and energy in event-by-event mode. The statistical model code PACE [19] is used to check the major decay channels in the $^{16}O + ^{194}Pt$ reaction at 96.0 MeV, and two xn channels were found to be dominant at this energy ($4n$ and $5n$ channels with abundances 32.4% and 55.8% of the total ER cross sections, respectively). The angular distributions are simulated for these two neutron evaporation channels and these are normalized (weighted-averaged) to obtain the total ER angular distribution for the $^{16}O + ^{194}Pt$ reaction at 96.0 MeV. Similar calculations are also performed for the $^{16,18}O + ^{198}Pt$ reactions. Hence, to extract T_{eff} for the $^{16,18}O + ^{198}Pt$ reactions using the $^{16}O + ^{194}Pt$ reaction, the total ER angular distributions are compared. The transmission efficiency (T_{eff}), calculated for the $^{16}O + ^{194}Pt$ reaction at $E_{lab} = 96$ MeV using the ER counts from the MWPC detector is found to be $1.22 \pm 0.17\%$. The circular exit aperture of the target chamber,
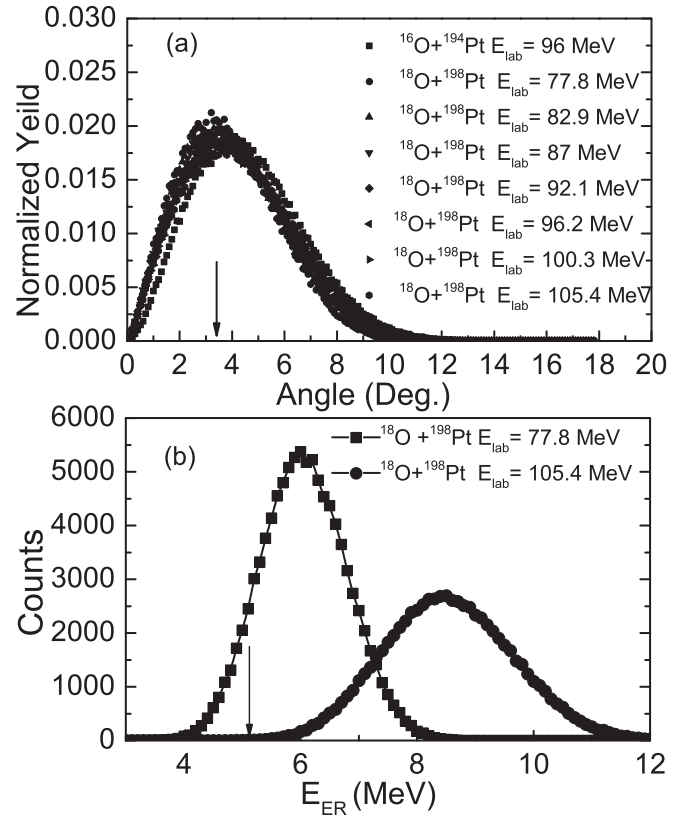
FIG. 2. (a) The normalized angular distributions of ERs from $^{16}O + ^{194}Pt$ and $^{18}O + ^{198}Pt$ reactions at different laboratory energies simulated using the Monte Carlo code TERS. The arrow at $3.35°$ indicates the angular acceptance of HYRA. (b) Energy distribution for $^{18}O + ^{198}Pt$ at lowest and highest energies using TERS. The arrow shows the energy threshold for ER in HYRA.

translating to an angle (polar) of $3.35°$, defined the angular acceptance of HYRA and is considered in the present procedure.

The total angular distributions of ERs for $^{18}O + ^{198}Pt$ reaction at different beam energies are shown in Fig. 2(a). For the purpose of comparison, the total number of ERs, i.e., areas under each curve, were kept the same in all cases. In this method, to get the estimated transmission efficiency, we assume that the HYRA acceptance in the charge state is nearly 100%, and the factor that causes a difference in transmission efficiency for different reactions is the angular distribution of the ERs as we carefully optimized the magnetic field values and gas pressure. Accordingly, a multiplication factor of 0.42 is obtained after multiplying the area under $3.35°$ for the $^{16}O + ^{194}Pt$ reaction to get the measured T_{eff} value (1.22%) for the same reaction. The same multiplication factor is used to get the T_{eff} values for the $^{16,18}O + ^{198}Pt$ reaction after getting the area under each curve. The extracted transmission efficiencies for the $^{16,18}O + ^{198}Pt$ systems are given in Table I at different beam energies.

B. ER cross sections

The ER cross sections are calculated using the expression

$$\sigma_{ER} = \frac{1}{T_{eff}} \left(\frac{Y_{ER}}{Y_M} \right) \left(\frac{d\sigma}{d\Omega} \right)_R \Omega_M, \tag{1}$$

TABLE I. Measured transmission efficiency of HYRA for the ^{16,18}O + ^{198}Pt reactions as a function of center-of-mass energy, $E_{c.m.}$.

^{16}O + ^{198}Pt			^{18}O + ^{198}Pt		
E_{cm} (MeV)	T_{eff} (%)	±error (%)	E_{cm} (MeV)	T_{eff} (%)	±error (%)
72.1	1.63	0.23	71.4	1.75	0.24
75.1	1.55	0.22	76.0	1.66	0.23
77.9	1.52	0.21	79.8	1.63	0.23
79.8	1.52	0.21	84.4	1.55	0.22
81.6	1.51	0.21	88.2	1.50	0.21
85.2	1.47	0.21	91.9	1.48	0.21
86.4	1.45	0.20	96.6	1.45	0.20
88.8	1.42	0.20			
91.1	1.41	0.19			
93.0	1.38	0.19			
94.8	1.37	0.19			
97.7	1.32	0.19			

where T_{eff} is the average HYRA transmission efficiency for ERs, Y_{ER} is the yield of ERs, Y_M is the geometric mean of the monitor yields, $(d\sigma/d\Omega)_R$ is the Rutherford cross section in the laboratory frame and Ω_M is the solid angle subtended by the monitors at the target. The Rutherford cross section in laboratory frame can be written as

$$\left(\frac{d\sigma}{d\Omega}\right)_R = 1.296 \left(\frac{Z_p Z_t}{E_{\text{lab}}}\right)^2 \left[\frac{1}{\sin^4\left(\frac{\theta}{2}\right)} - 2\left(\frac{M_p}{M_t}\right)^2\right], \quad (2)$$

where Z_p, Z_t, M_p, and M_t are the atomic numbers and mass numbers of the projectile and target respectively. E_{lab} and θ are the energy of the incident particle and scattering angle of the projectile-like particles in the laboratory frame of reference respectively. While extracting the ER cross sections, the energy loss of the beam and evaporation residues in the target foil are taken into account.

C. Experimental results

The transmission efficiencies at different energies are used in Eq. (1) to obtain the ER cross sections. Along with the angular distributions, energy distribution calculations are also done using the code TERS to get the percentage of counts which come below the energy threshold of ^{16,18}O + ^{198}Pt reactions at each energy. Energy thresholds are calculated by taking into account the energy losses in the helium gas at 0.15 torr and MWPC (Mylar, isobutane) for ^{16,18}O + ^{198}Pt and the calculated values are 4.6 and 5.2 MeV respectively for both the reactions. Figure 2(a) show the energy distribution spectra for both the reactions along with the angular acceptance of HYRA, and Fig. 2(b) shows the corresponding spectra for ^{18}O + ^{198}Pt at lowest and highest beam energies along with energy threshold (E_{th}). It is found that for both of the reactions about 14% of counts at the lowest and 0.03% at the highest energy are coming below the energy threshold, and these values are further incorporated in the final measured cross sections. The overall errors in the estimated ER cross sections are less than 20%, out of which T_{eff} contributes the maximum. The excitation functions of the measured ER cross
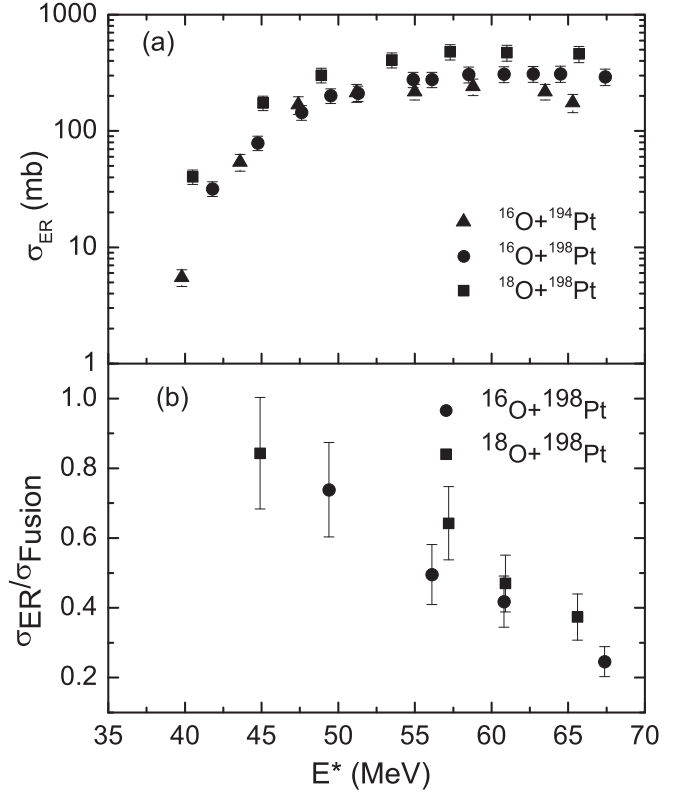
FIG. 3. Variation of (a) ER cross section and (b) ER survival probability with excitation energy for ^{16,18}O + ^{198}Pt systems.

sections for the ^{16,18}O + ^{198}Pt reactions are shown in Fig. 3(a). The ER excitation function for the previously measured [13] ^{16}O + ^{194}Pt system is also shown in this figure for the sake of comparison. The data show that ER cross section increases with increasing values of N/Z of the compound nuclei in an isotopic chain. A similar observation was made earlier for other systems [20,21]. The survival probabilities of the compound nuclei ^{214}Rn and ^{216}Rn formed in the ^{16,18}O + ^{198}Pt reactions are next shown in Fig. 3(b). An increase in survival probability with neutron number in the CN is also observed here. The measured ER cross sections for the different systems under study are given in Table II.

IV. STATISTICAL MODEL CALCULATION

The decay channels of an excited compound nucleus considered in the present statistical model calculation are emission of light particles (neutron, proton, and α) and giant dipole resonance (GDR) γ rays in addition to fission. Particle and GDR γ decay widths are obtained from the Weisskopf formula [7,22]. An important input to statistical model calculations is the level density parameter which is used to obtain various decay widths. We take the level density parameter from the work of Ignatyuk *et al.* [23] where the effect of shell structure in reducing the level density at low excitation energies is included and is given as follows:

$$a(\mathbf{q}, U) = \tilde{a}(\mathbf{q})\left[1 + \frac{f(U)}{U}\delta W\right],$$
$$f(U) = 1 - \exp(-U/E_D), \quad (3)$$

TABLE II. Measured ER cross sections (σ_{ER}) for the ^{16,18}O + ^{198}Pt reactions as a function of E_{lab}, $E_{c.m.}$, and E^*.

^{16}O + ^{198}Pt					^{18}O + ^{198}Pt				
E_{lab} (MeV)	E_{cm} (MeV)	E^* (MeV)	σ_{ER} (mb)	$\pm$error (mb)	E_{lab} (MeV)	E_{cm} (MeV)	E^* (MeV)	σ_{ER} (mb)	$\pm$error (mb)
78.0	72.1	41.8	31.9	4.6	77.8	71.4	40.5	40.4	5.7
81.1	75.1	44.8	78.9	11.1	82.8	76.0	45.1	174.7	25.0
84.2	77.9	47.6	144.6	20.8	86.9	79.8	48.9	301.9	43.6
86.2	79.8	49.5	201.2	29.3	92.0	84.4	53.5	408.4	59.6
88.3	81.6	51.3	211	31.2	96.0	88.2	57.3	480	72.1
92.0	85.2	54.9	277	41.7	100.3	91.9	61.0	472	74.1
93.4	86.4	56.1	278	41.9	105.4	96.6	65.7	459.7	73.5
96.0	88.8	58.5	307	47.5					
98.6	91.1	60.8	308	48.0					
100.5	93.0	62.7	310.6	48.2					
102.5	94.8	64.5	311	49.5					
105.6	97.7	67.4	293.3	46.9					

where U is the thermal energy of the compound nucleus, δW is the shell correction energy taken from the difference between the experimental and liquid drop model masses, E_D accounts for the rate at which the shell effect melts away with increase of excitation energy, and $\tilde{a}(\mathbf{q})$ is the asymptotic value to which the level density parameter approaches with increasing excitation energy of the compound nucleus. $\tilde{a}$ depends upon the nuclear mass number and the shape, specified by the collective coordinates $\mathbf{q}$, in a fashion similar to the liquid drop model of mass and its values are taken from Ref. [24].

We first calculate the ER cross sections using the following form of Bohr-Wheeler fission width [25],

$$\Gamma_{BW} = \frac{\hbar\omega_g}{2\pi} \exp\left(\frac{-V_B}{T}\right), \qquad (4)$$

where ω_g is the frequency of the harmonic oscillator potential which has the same curvature as that of the potential energy profile at the ground state of the CN. The fission barrier V_B is obtained from the finite-range liquid drop model (FRLDM) [26] potential which includes the rotational energy of the compound nucleus obtained using the shape-dependent rigid body moment of inertia. It may be remarked here that Eq. (4) includes the classical phase space associated with the collective motion at the ground state [27]. Collective enhancement in nuclear level density (CELD) due to vibrational and rotational degrees of freedom has also been suggested earlier [28,29]. Since the Bohr-Wheeler fission width is given by the ratio of the phase spaces at the saddle and at the ground state configurations of the CN, CELD will impact the available phase spaces at the saddle and ground states quite differently because of the large deformation at the saddle [30]. The damping of CELD with increasing excitation energy is predicted to depend on nuclear deformation [28,29] which, however, contrasts with the observation that a deformation-independent damping factor better fits the experimental data [30]. Moreover, we use Kramers' fission width in the later part of the present work, which is obtained from classical considerations, and hence CELD cannot be directly included in Kramers' fission width. Due to such reasons, we do not include CELD in calculating fission widths in the present work. In this context, we may

further add that CELD can also impact the various particle and γ-decay widths since it modifies the level densities of the parent and the daughter nuclei. However, it has been recently observed that collectivity does not have a significant effect on neutron evaporation spectra from a near-spherical compound nucleus [31]. It has also been observed in a multidimensional Langevin dynamical calculation that the fission excitation function of a nearly spherical CN is not sensitive to the inclusion of CELD in calculating the widths of evaporation channels [32]. Since the compound nuclei considered in the present work are also nearly spherical, we expect the CELD effect in particle decay widths will not be significant, and hence it is not included in the present work.

In the statistical model calculation, a compound nucleus is followed in time over small time steps and, at each time step the fate of the compound nucleus is decided by a Monte Carlo sampling using the particle, γ, and the fission widths [33]. In the event of a particle or γ emission, the residual nucleus is appropriately redefined and its excitation energy and angular momentum adjusted through another Monte Carlo sampling procedure. The process continues till either the compound nucleus undergoes fission or an evaporation residue is formed. The initial spin of the CN is chosen from a Monte Carlo sampling of the spin distribution which corresponds to the fusion cross section in the entrance channel. Spin distributions are obtained from the coupled channel code CCFULL [34] where the depth of the potential V_0 is adjusted at each beam energy to fit the excitation function of experimental fusion cross sections while keeping the values of the parameters r_0 and a_0 fixed. Coupling of the rotational states of the target is considered in the calculations. Figures 4(a) and 4(b) show the experimental fusion cross section as a function of E_{cm} along with the CCFULL results for the ^{16,18}O + ^{198}Pt systems. The fission cross sections for the same reactions are taken from Ref. [35].

The ER excitation functions for the ^{16,18}O + ^{198}Pt systems calculated using the Bohr-Wheeler fission width with FRLDM fission barriers are given in Fig. 5 along with the experimental data. The calculated values overestimate the ER cross sections for both the reactions. No shell correction is applied to the fission barrier in this calculation. We next add shell correction
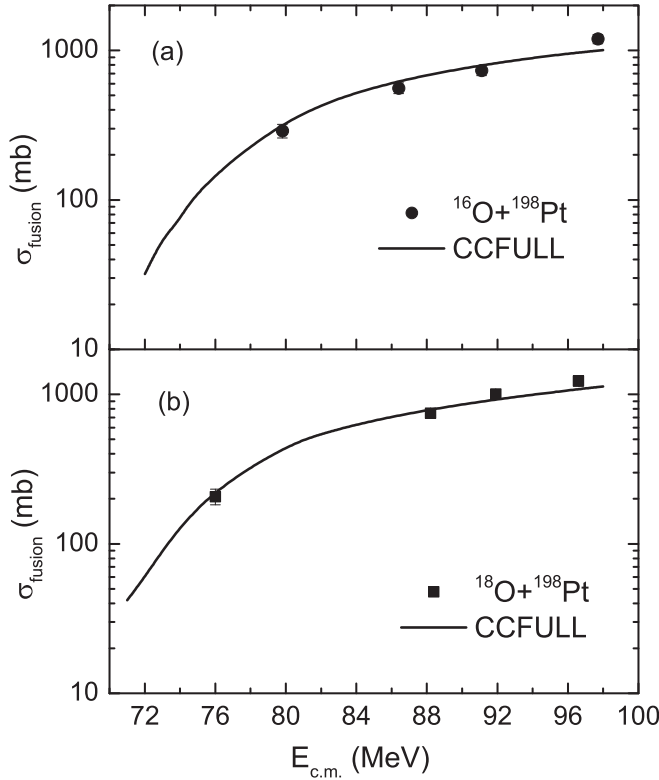
FIG. 4. (a) Fusion cross section for ^{16}O + ^{198}Pt. (b) Fusion cross section for ^{18}O + ^{198}Pt. The total fusion cross sections calculated using the coupled-channels code CCFULL are also shown.
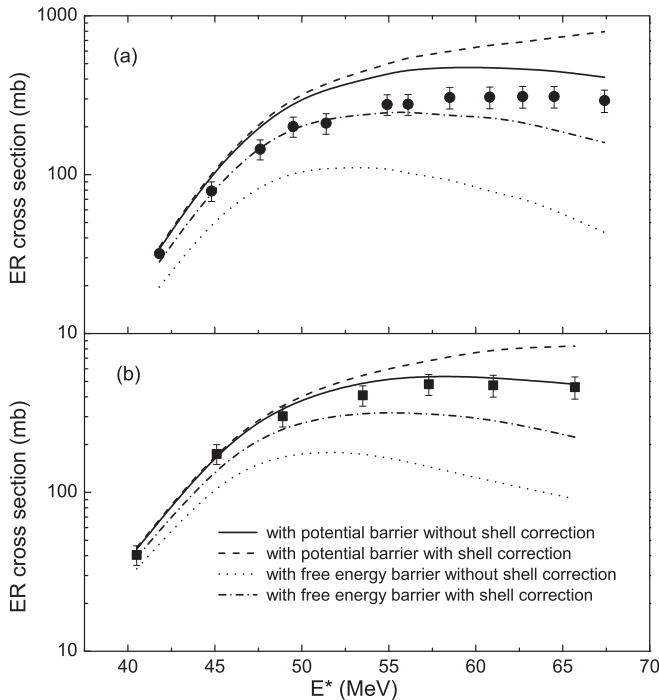
FIG. 5. Calculated ER excitation functions for different choices of fission barrier along with the experimental ER cross sections: (a) ^{16}O + ^{198}Pt (full circles), (b) ^{18}O + ^{198}Pt (full squares).

to the FRLDM barrier as [36]

$$V_B^{\text{shell}}(T) = V_B^{FRLDM} - \delta W \exp\left(-\frac{U}{E_D}\right) \quad (5)$$

and use the shell-corrected barriers to calculate the ER excitation functions. Figure 5 shows the results. Shell correction increases the height of the fission barriers for the present compound nuclei, and consequently the ER cross sections also increase as we find in Fig. 5.

It has been pointed out earlier that the driving force in a thermodynamical system like a hot nucleus is provided by the free energy rather than the potential energy of the system [25,37,38]. We therefore use free energy for subsequent statistical model calculations. The free energy F is given in the Fermi gas model as

$$F(\mathbf{q}, T) = V(\mathbf{q}) - \tilde{a}(\mathbf{q})T^2 \quad (6)$$

where $V(\mathbf{q})$ is the FRLDM potential. The Bohr-Wheeler fission width in free energy profile is therefore given as [25]

$$\Gamma_{BW}^F = \frac{\hbar\omega_g(T)}{2\pi} \exp\left(\frac{-F_B(T)}{T}\right) \quad (7)$$

where the frequency $\omega_g(T)$ and the fission barrier $F_B(T)$ now depend on temperature. Evaporation residue excitation functions calculated with free energy fission barriers are also given in Fig. 5 for both the reactions under consideration. We next consider the shell-corrected fission barrier in free energy, which is given as [39]

$$F_B^{\text{shell}}(T) = F_B^{\text{no-shell}}(T) - \delta W \exp\left(-\frac{U}{E_D}\right), \quad (8)$$

and evaporation residue excitation functions calculated with shell corrected free energy fission barriers are also given in Fig. 5. The free energy fission barriers are lower than the potential energy barriers [25], and consequently the calculated ER cross sections with free energy barriers are smaller than those obtained with potential barriers.

We observe in Fig. 5 that statistical model calculations using Bohr-Wheeler fission width with shell-corrected free energy fission barrier underestimate ER cross sections, particularly at higher excitation energies. This suggests a fission hindrance due to the presence of a dissipative force in fission dynamics. In what follows, we therefore use the fission width due to Kramers where the effect of dissipation in fission dynamics is included [6]. The Kramers' fission width is given as [6,25]

$$\Gamma_K = \frac{\hbar\omega_g(T)}{2\pi} \exp\left(\frac{-F_B}{T}\right) \left(\sqrt{1 + \left(\frac{\beta}{2\omega_s(T)}\right)^2} - \frac{\beta}{2\omega_s(T)}\right), \quad (9)$$

where β is the dissipation coefficient. In the above equation, $\omega_s(T)$ is defined similarly as $\omega_g(T)$ but at the saddle configuration. The Kramers' fission width of Eq. (9) represents a stationary fission rate which is reached after an initial delay or the transient time. This is taken into account in the statistical model calculation by using the following parametrized form of the time-dependent fission width [40]:

$$\Gamma_f(t) = \Gamma_K[1 - \exp(-2.3t/\tau_f)], \quad (10)$$

where the transient time τ_f is given as

$$\tau_f = \frac{\beta}{2\omega_g^2} \ln \left(\frac{10 F_B}{T} \right). \qquad (11)$$

It may be pointed out here that Eq. (9) represents the fission rate when the fission dynamics is restricted to only one dimension (elongation). Consideration of larger number of collective coordinates including various shape and the orientation (K) degrees of freedom to describe fission dynamics is expected to modify the above mentioned fission width. The projection of the angular momentum vector of the CN along the symmetry axis is denoted by K here and Eq. (9) represents the fission width for $K = 0$. The Bohr-Wheeler fission width modified to include the K degrees of freedom is given in Ref. [41] and the effect of the modification is found to reduce the fission width compared to the $K = 0$ case [25]. On the other hand, fission widths obtained from Langevin dynamical calculations are found to increase with increase in the number of the shape degrees of freedom [42]. Though the Kramers' fission width for multidimensional fission dynamics is given in Ref. [43], evaluation of its value requires numerical computation of the potential landscape in multiple dimensions, which is beyond the scope of the present statistical model calculation. Clearly, the dissipation strength obtained from fitting experimental data depends on the choice of the collective variables to describe the dynamics of fission. We therefore restrict ourselves to the simplest one-dimensional model of fission, and the fitted values of β will be understood in the context of the aforementioned model.

We next calculate evaporation residue cross sections using Kramers' fission width with the shell-corrected free energy fission barrier for different values of the dissipation coefficient (β) for both the reactions under study, and the results are given in Fig. 6 along with the experimental values. It is observed that good overall fits to the experimental excitation functions can be obtained with $\beta \sim (0$–$1) \times 10^{21}$ s^{-1} for the reaction ^{16}O + ^{198}Pt forming the compound nucleus ^{214}Rn and $\beta \sim (0.5$–$1.5) \times 10^{21}$ s^{-1} for ^{18}O + ^{198}Pt leading to the compound nucleus ^{216}Rn. While ER cross sections at low excitation energies can be fitted with smaller values of β, larger β values are necessary at higher excitations.

The dissipation coefficient β represents the irreversible energy flow from the collective fission degrees of freedom to intrinsic nuclear excitation and is a bulk property of a nucleus. However, the strength of β derived from fitting experimental data not only represents the dissipation but also accounts for other features which are not included in statistical model calculations. We have already discussed two such aspects in the earlier part of the present section, namely the effect of collective excitations in level density and the role of collective degrees of freedom other than elongation, which are not included in the present calculation. Due to such reasons, the derived β values for different nuclei may differ, which we find in the present work.

It may further be pointed out here that the strength of β obtained from fitting experimental data necessarily depends on the fission barrier height in the fission width expression.
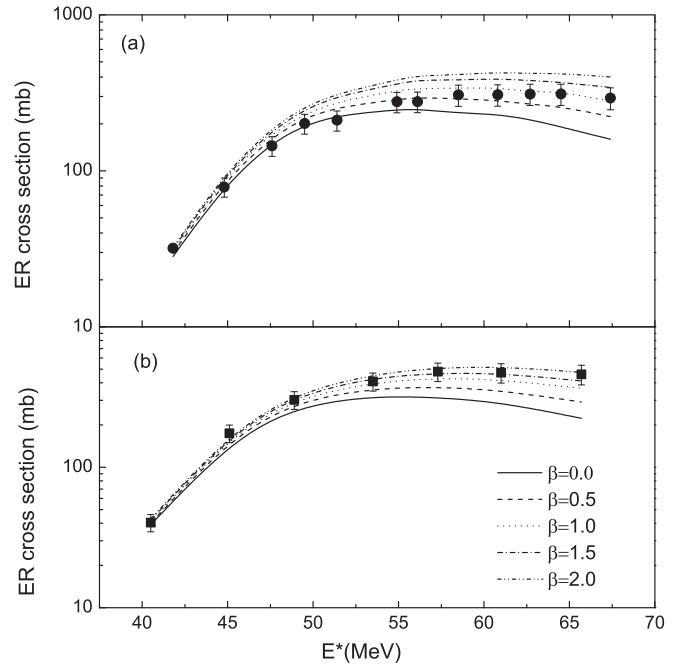
FIG. 6. Calculated ER excitation functions for different values of β (in units of 10^{21} s^{-1}) along with the experimental values: (a) ^{16}O + ^{198}Pt (full circles), (b) ^{18}O + ^{198}Pt (full squares).

As evident from Fig. 5, larger values of β will be required to fit ER cross sections if free energy fission barriers without shell correction are used in statistical model calculation. In fact, β values in the range of $(1$–$5) \times 10^{21}$ s^{-1} were found to be necessary in order to fit excitation functions of pre-scission neutron multiplicity for the same systems in a previous work [11]. Free energy fission barriers without shell correction were used in the above work. We therefore plan to perform simultaneous analysis of ER cross section and pre-scission neutron multiplicity of various systems using the shell-corrected free energy fission barrier in a future work.

V. SUMMARY AND DISCUSSIONS

We have presented experimental evaporation residue cross section data for the ^{16,18}O + ^{198}Pt reactions forming ^{214,216}Rn compound nuclei which are measured at excitation energies in the range of 40–68 MeV. Comparison of the survival probabilities of the compound nuclei derived from the experimental data shows that ^{216}Rn with neutron number $N = 130$ has higher stability against fission compared to ^{214}Rn with $N = 128$.

Statistical model analysis of ER cross sections shows that a dissipation in fission dynamics is necessary to fit the experimental data. The dissipation strength β required to fit the experimental data is found to increase with increase of CN excitation energy. The best-fit dissipation strengths lie in the ranges $(0$–$1) \times 10^{21}$ s^{-1} and $(0.5$–$1.5) \times 10^{21}$ s^{-1} for the compound nuclei ^{214}Rn and ^{216}Rn respectively. In a recent multidimensional Langevin dynamical calculation including the orientation degree of freedom, reasonable agreement with

experimental observables is obtained for the compound nuclei ^{206,210}Po [44]. The chaos-weighted one-body dissipation from Ref. [45] used in this work is shape dependent and varies in the range $(0-3) \times 10^{21}$ s^{-1} between the ground state and the saddle configuration. The shape-independent β values obtained in the present work are thus in the same range as to those employed in the multidimensional Langevin dynamical calculation.

[1] P. Frobrich and I. I. Gontchar, Nucl. Phys. A **563**, 326 (1993).

[2] W. Ye, Phys. Rev. C **81**, 011603 (2010).

[3] Y. Oganessian, J. Phys. (London) G **34**, R165 (2007).

[4] M. Thoennessen and G. F. Bertsch, Phys. Rev. Lett. **71**, 4303 (1993).

[5] N. Bohr and J. A. Wheeler, Phys. Rev. **56**, 426 (1939).

[6] H. A. Kramers, Physica (Amsterdam) **7**, 284 (1940).

[7] I. Dioszegi, N. P. Shaw, I. Mazumdar, and A. Hatzikoutelis, and P. Paul, Phys. Rev. C **61**, 024613 (2000).

[8] P. N. Nadtochy, E. G. Ryabov, A. E. Gegechkori, Yu. A. Anischenko, and G. D. Adeev, Phys. Rev. C **85**, 064619 (2012).

[9] R. N. Sagaidak, and A. N. Andreyev, Phys. Rev. C **79**, 054613 (2009).

[10] V. Singh, B. R. Behera, M. Kaur, A. Kumar, K. P. Singh, N. Madhavan, S. Nath, J. Gehlot, G. Mohanto, A. Jhingan, Ish Mukul, T. Varughese, J. Sadhukhan, S. Pal, S. Goyal, A. Saxena, S. Santra, and S. Kailas, Phys. Rev. C **89**, 024609 (2014).

[11] R. Sandal, B. R. Behera, V. Singh, M. Kaur, A. Kumar, G. Singh, K. P. Singh, P. Sugathan, A. Jhingan, K. S. Golda, M. B. Chatterjee, R. K. Bhowmik, D. Siwal, S. Goyal, S. Mandal, E. Prasad, K. Mahata, A. Saxena, J. Sadhukhan, and S. Pal, Phys. Rev. C **87**, 014604 (2013).

[12] Rohit Sandal, B. R. Behera, N. Madhavan, S. Nath, J. Gehlot, A. Jhingan, K. S. Golda, H. Singh, V. Singh, A. Kumar, M. Kaur, G. Kaur, P. Sharma, S. Mandal, S. Verma, E. Prasad, K. M. Varier, A. M. Vinodkumar, and A. Saxena, Proc. DAE Symp. Nucl. Phys. **57**, 532 (2012).

[13] E. Prasad, K. M. Varier, N. Madhavan, S. Nath, J. Gehlot, S. Kalkal, J. Sadhukhan, G. Mohanto, P. Sugathan, A. Jhingan, B. R. S. Babu, T. Varughese, K. S. Golda, B. P. Ajith Kumar, B. Satheesh, S. Pal, R. Singh, A. K. Sinha, and S. Kailas, Phys. Rev. C **84**, 064606 (2011).

[14] N. Madhavan *et al.*, Pramana J. Phys. **75**, 317 (2010).

[15] S. Nath, a Monte Carlo code to model ion transport in dilute gas medium (unpublished).

[16] E. T. Subramanium, B. P. Ajith Kumar and R. K. Bhowmik, CANDLE: Collection and Analysis of Nuclear Data using Linux Network (unpublished).

[17] S. Nath, P. V. Madhusudhana Rao, S. Pal, J. Gehlot, E. Prasad, G. Mohanto, S. Kalkal, J. Sadhukhan, P. D. Shidling, K. S. Golda, A. Jhingan, N. Madhavan, S. Muralithar, and A. K. Sinha, Phys. Rev. C **81**, 064601 (2010).

[18] S. Nath, Comput. Phys. Commun. **180**, 2392 (2009).

[19] A. Gavron, Phys. Rev. C **21**, 230 (1980).

[20] R. J. Charity, J. R. Leigh, J. J. M. Bokhorst, A. Chatterjee, G. S. Foote, D. J. Hinde, J. O. Newton, S. Ogaza, and D. Ward, Nucl. Phys. A **457**, 441 (1986).

[21] R. Rafiei, R. G. Thomas, D. J. Hinde, M. Dasgupta, C. R. Morton, L. R. Gasques, M. L. Brown, and M. D. Rodriguez, Phys. Rev. C **77**, 024606 (2008).

[22] P. Fröbrich and I. I. Gontchar, Phys. Rep. **292**, 131 (1998).

[23] A. V. Ignatyuk, G. M. Smirenkin, and A. Tishin, Sov. J. Nucl. Phys. **21**, 255 (1975).

[24] W. Reisdorf, Z. Phys. A **300**, 227 (1981).

[25] J. P. Lestone and S. G. McCalla, Phys. Rev. C **79**, 044611 (2009).

[26] A. J. Sierk, Phys. Rev. C **33**, 2039 (1986).

[27] V. M. Strutinsky, Phys. Lett. B **47**, 121 (1973).

[28] S. Bjornholm, A. Bohr, and B. R. Mottelson, in *Proceedings of the International Conference on the Physics and Chemistry of Fission*, Rochester, 1973, Vol. 1 (IAEA, Vienna, 1974), p. 367.

[29] G. Hansen and A. S. Jensen, Nucl. Phys. A **406**, 236 (1983).

[30] A. R. Junghans, M. de Jong, H.-G. Clerc, A. V. Ignatyuk, G. A. Kudyaev, and K.-H. Schmidt, Nucl. Phys. A **629**, 635 (1998).

[31] P. Roy, K. Banerjee, M. Gohil, C. Bhattacharya, S. Kundu, T. K. Rana, T. K. Ghosh, G. Mukherjee, R. Pandey, H. Pai, V. Srivastava, J. K. Meena, S. R. Banerjee, S. Mukhopadhyay, D. Pandit, S. Pal, and S. Bhattacharya, Phys. Rev. C **88**, 031601(R) (2013).

[32] A. V. Karpov, P. N. Nadtochy, E. G. Ryabov, and G. D. Adeev, J. Phys. G: Nucl. Part. Phys. **29**, 2365 (2003).

[33] G. Chaudhuri and S. Pal, Phys. Rev. C **65**, 054612 (2002).

[34] K. Hagino, N. Rowley, and A. T. Kruppa, Comput. Phys. Commun. **123**, 143 (1999).

[35] Rohit Sandal, B. R. Behera, V. Singh, M. Kaur, S. Mandal, S. Kalkal, D. Siwal, S. Goyal, E. Prasad, P. Sugathan, A. Jhingan, and A. Saxena, Proc. DAE Symp. Nucl. Phys. **57**, 534 (2012).

[36] Y. Aritomo, Nucl. Phys. A **780**, 222 (2006).

[37] A. Bohr and B. R. Mottelson, *Nuclear Structure*, Vol. II (Benjamin, London, 1975).

[38] E. G. Ryabov, A. V. Karpov, P. N. Nadtochy, and G. D. Adeev, Phys. Rev. C **78**, 044614 (2008).

[39] Y. Aritomo, T. Wada, M. Ohta, and Y. Abe, Phys. Rev. C **59**, 796 (1999).

[40] K. H. Bhatt, P. Grange, and B. Hiller, Phys. Rev. C **33**, 954 (1986).

[41] J. P. Lestone, Phys. Rev. C **59**, 1540 (1999).

[42] P. N. Nadtochy, A. Kelic, and K.-H. Schmidt, Phys. Rev. C **75**, 064614 (2007).

[43] J.-S. Zhang, and H. A. Weidenmüller, Phys. Rev. C **28**, 2190(R) (1983).

[44] C. Schmitt, K. Mazurek, and P. N. Nadtochy, Phys. Lett. B **737**, 289 (2014).

[45] G. Chaudhuri and S. Pal, Phys. Rev. C **63**, 064603 (2001).